Biochimica et Biophysica Acta, 944 (1988) 108–111
Elsevier

BBA 70577

BBA Report

Spatio-temporal patterns in the fluid-mosaic model of membranes

Peter Fromherz

Abteilung Biophysik der Universität Ulm, Ulm-Eselsberg (F.R.G.)

(Received 6 June 1988)

Key words: Membrane protein; Membrane potential; Electrical interaction; Ion channel; Morphogenesis selforganization

The lateral distribution of integral proteins in a fluid membrane is studied in a phenomenological model. The electrical interaction of the proteins (forming ion channels and bearing electrophoretic charges) with the membrane potential is considered. Stationary and oscillatory patterns appear far from electrochemical equilibrium under conditions which may well exist in natural membranes.

Lateral structures in biological membranes may appear to be incompatible with the model of a 'fluid-mosaic' of proteins floating freely in a liquid lipid bilayer [1]. However, a homogeneous fluid mosaic of ion channels [2,3] with electrophoretic charges [4,5] may become structurally unstable as a result of its coupling to the electrical membrane potential [6,12]. The nonlinear dynamics of two kinds of mobile charged channels in a cable is studied by numerical integration. Far from electrochemical equilibrium the fluid mosaic forms coherent patterns such as stationary, oscillatory and solitary waves.

Let us consider a cylinder made of a lipid bilayer embedded in electrolyte. The membrane potential V_M as a function of space x and time t is governed by the balance of current densities according to the cable equation [7]:

$$C_M \cdot \frac{\partial V_M}{\partial t} = \frac{1}{R_l} \cdot \frac{\partial^2 V_M}{\partial x^2} - \Lambda_A \cdot N_A \cdot (V_M - E_A^0) - \Lambda_B \cdot N_B \cdot (V_M - E_B^0) \quad (1)$$

The conductivity of the membrane due to channels A and B is expressed by the conductances Λ_A and Λ_B and by the densities per unit length N_A and N_B. E_A^0 and E_B^0 are the reversal potentials. R_l is the resistance per unit length of the core, neglecting the resistance of the bath. C_M is the capacitance per unit length.

The density of the channels may change due to lateral diffusion and electrophoretic drift:

$$\frac{\partial N_A}{\partial t} = D_A \cdot \frac{\partial}{\partial x}\left[\frac{\partial N_A}{\partial x} + N_A \cdot \frac{q_A}{kT} \cdot \frac{\partial V_M}{\partial x}\right] \quad (2)$$

$$\frac{\partial N_B}{\partial t} = D_B \cdot \frac{\partial}{\partial x}\left[\frac{\partial N_B}{\partial x} + N_B \cdot \frac{q_B}{kT} \cdot \frac{\partial V_M}{\partial x}\right] \quad (3)$$

D_A and D_B are the diffusion coefficients. q_A and q_B are electrophoretic charges exposed to the core. kT is the thermal energy. The number of A- and B-channels is constant as given by the average densities $\bar{N}_A$ and $\bar{N}_B$ in a cable of length l_M. For tight ends the constraints are $\partial V_M/\partial x = \partial N_A/\partial x = \partial N_B/\partial x = 0$ at $x = 0, l_M$.

The coupled nonlinear Eqns. 1–3 describe an ideal fluid mosaic of charged channels on a phenomenological level with neglect of short range interactions.

Correspondence: P. Fromherz, Abteilung Biophysik der Universität Ulm, D-7900 Ulm-Eselsberg, F.R.G.

Numerical integrations of Eqns. 1–3 are shown in Fig. 1 for selected parameters, starting from the homogeneous stationary state $N_A = \bar{N}_A$, $N_B = \bar{N}_B$ with a small symmetrical perturbation.

Space is scaled by the length constant $\xi = (R_I \cdot \bar{G})^{-1/2}$ with the conductivity $\bar{G} = \Lambda_A \cdot \bar{N}_A + \Lambda_B \cdot \bar{N}_B$. The length of the cable is $l_M/\xi = 10$. Time is scaled by three time constants $\tau_V = C_M/\bar{G}$, $\tau_A = \xi^2/D_A$ and $\tau_B = \xi^2/D_B$. The potential relaxes fast with respect to the motion of the A-channels with $\tau_V = \tau_A/100$. The A-channels move faster than the B-channels with $\tau_A = \tau_B/10$. The composition of the membrane is characterized by the fractions of conductivity $\alpha_A = \Lambda_A \cdot \bar{N}_A/\bar{G}$ and $\alpha_B = \Lambda_B \cdot \bar{N}_B/\bar{G}$ with $\alpha_A = \alpha_B = 0.5$. The coupling of the channels to the potential is characterized by the 'drive' parameters $\epsilon_A = (E_B^0 - E_A^0) \cdot q_A/kT$ and $\epsilon_B = (E_A^0 - E_B^0) \cdot q_B/kT$ with $\epsilon_A = 20$ and $\epsilon_B = 8, -8, -20$ and -100.

Let us consider a qualitative interpretation of the patterns.

For convenience let $E_A^0 = 50$ mV and $E_B^0 = -50$ mV. With this choice an electrical current flows inwards through an A-channel such that a positive local perturbation of the potential is induced. Through a B-channel the current flows outwards with a concomitant negative local perturbation of the potential.

A drive parameter $\epsilon_A = 20$ corresponds to a negative charge $q_A = -5e_0$ (e_0 elementary charge, $kT/e_0 = 25$ mV). Each A-channel is attracted by other A-channels and repelled by the B-channels due to the lateral electrical fields as created by the lateral spread in the core of inward and outward current, respectively.

A drive parameter $\epsilon_B = 8$ corresponds to a positive charge $q_B = 2e_0$. Each B-channel is attracted by other B-channels and repelled by the A-channels. 'B likes B, B dislikes A' with 'A likes A, A dislikes B'. The fluid mosaic decomposes into 'droplets' along the cable rich in A- and B-channels (Fig. 1a). $\epsilon_B = -8$ corresponds to a negative

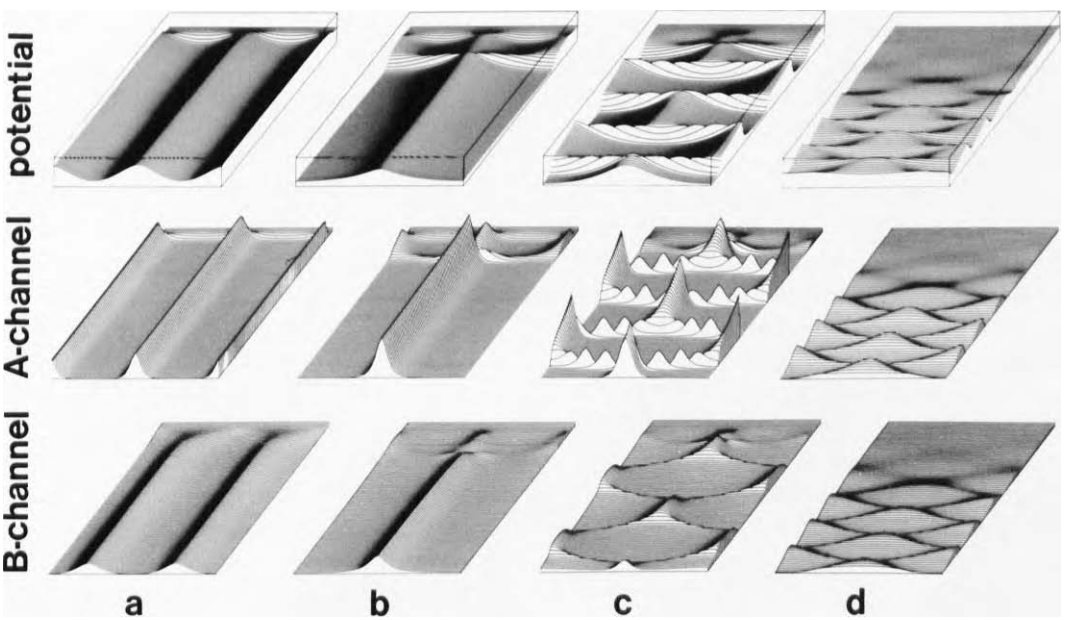

Fig. 1. Spatiotemporal patterns in a cable. Top row: membrane potential V_M. Second row: density N_A of A-channels. Bottom row: density N_B of B-channels. In each figure space is plotted from left to right and time from back to front. The length equals ten electrical length constants: $l_M = 10\xi$. The total time equals seven time constants of the B-channels: $t_{tot} = 7\tau_B$. In the top row the upper and lower plane mark the reversal potentials E_A^0 and E_B^0, respectively. The levels of the average densities $\bar{N}_A$ and $\bar{N}_B$ are indicated by the initial profiles. The four columns refer to (a) $\epsilon_B = 8$, (b) $\epsilon_B = -8$, (c) $\epsilon_B = -20$ and (d) $\epsilon_B = -100$. The other parameters are $\epsilon_A = 20$, $\alpha_A = \alpha_B = 0.5$, $\tau_A = \tau_B/10$ and $\tau_V = \tau_A/100$. Forward integration is applied using an Euler algorithm in real space for 51 lattice points. Increments in space and time are $\Delta x = \xi/5$ and $\Delta t = \tau_V/100$. At the start the number of A-channels in the central lattice point is enhanced by 20%. The symmetrical perturbation triggers symmetrical patterns.

charge $q_B = -2e_0$. Each B-channel is repelled by other B-channels and attracted by the A-channels. 'B dislikes B moderately, B likes A moderately' with 'A likes A, A dislikes B'. A droplet of A-channels induces a droplet of B-channels (Fig. 1b). $\epsilon_B = -20$ corresponds to $q_B = -5e_0$. 'B dislikes B hesitantly, B likes A hesitantly' with 'A likes A, A dislikes B'–taking into account the time constants. The delayed attraction of the B-channels is so effective that an A-droplet spreads and splits at a certain threshold into two fragments which move at constant shape and velocity (Fig. 1c). Finally $\epsilon_B = -100$ corresponds to $q_B = -25e_0$. 'B dislikes B hesitantly but intensively, B likes A hesitantly but intensively' with 'A likes A, A dislikes B'. Formation and decay of droplets occur as a smooth oscillation due to the strong interaction of the damping B-channels (Fig. 1d).

An accumulation of channels pulls the membrane potential towards the corresponding reversal potential (Fig. 1, top row). Inward and outward currents through accumulations of A- and B-channels are connected to vortices by the currents along core and bath. Oscillating patterns imply oscillating vortices.

A systematic assignment of the patterns to the parameters is obtained from linear analysis.

Let us consider periodic perturbations of the stationary homogeneous state as $(N_A - \bar{N}_A)/\bar{N}_A = a_q \cdot \cos q \cdot x/\xi$, $(N_B - \bar{N}_B)/\bar{N}_B = b_q \cdot \cos q \cdot x/\xi$ and $(V_M - \bar{E}_R)/(E_A^0 - E_B^0) = v_q \cos q \cdot x/\xi$. $q = n\pi\xi/l_M$ is the normalized wavenumber with the order of the eigenmodes $n = 1, 2, \ldots$ $\bar{E}_R = \alpha_A E_A^0 + \alpha_B E_B^0$ is the average resting potential. Insertion of this ansatz into Eqns. 1–3 leads to a linearized dynamics of the amplitudes a_q, b_q and v_q. In case of fast electrical relaxation the potential is defined by the channel densities as $v_q = \alpha_A \cdot \alpha_B \cdot (a_q - b_q)/(1 + q^2)$. The linear rate equations for the channel modes are then:

$$da_q/dt = (q^2/4\tau_A)[(P_A - 4) \cdot a_q - P_A \cdot b_q] \quad (4)$$

$$db_q/dt = (q^2/4\tau_B)[-P_B \cdot a_q + (P_B - 4) \cdot b_q] \quad (5)$$

The 'pump' parameters P_A and P_B are defined as $P_A = 4 \cdot \epsilon_A \cdot \alpha_A \cdot \alpha_B/(1 + q^2)$ and $P_B = 4 \cdot \epsilon_B \cdot \alpha_B \cdot \alpha_A/(1 + q^2)$. The diagonals of Eqns. 4 and 5 refer to the selfinteraction of the modes of A- and B-channels as mediated by the potential, the off-diagonals refer to the cross interactions.

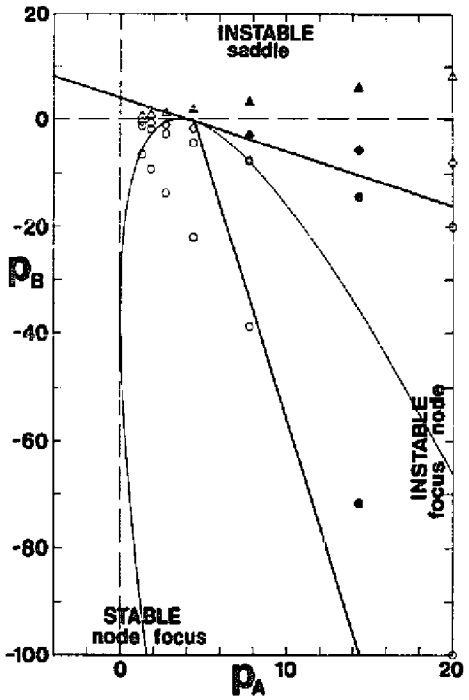

Fig. 2. Phase plane of the parameters P_A and P_B for a ratio of time constants $\tau_B/\tau_A = 10$. The phase points for $l_M/\xi = 10$, $\epsilon_A = 20$ and $\epsilon_B = 8, -8, -20, -100$ are marked by triangles, squares, hexagons and circles, respectively, with respect to the even modes $n = 2, 4, 6, 8, 12$ as aligned along rays from right to left. Growing modes are marked by full symbols, decaying modes and the virtual mode $n = 0$ by open symbols.

Stability and instability of the fluid mosaic are indicated by the coefficients of Eqns. 4 and 5 as illustrated in the phase plane P_A/P_B of Fig. 2. The homogeneous cable is stable for negative trace and positive determinant ($\mathrm{Tr} < 0$, $\Delta > 0$) as a focus ($\mathrm{Tr}^2 < 4\Delta$) or node ($\mathrm{Tr}^2 > 4\Delta$). The homogeneous cable is unstable for positive trace and positive determinant ($\mathrm{Tr} > 0$, $\Delta > 0$) as node or focus and for negative determinant ($\Delta < 0$) as a saddle.

Let us assign the patterns of nonlinear dynamics (Fig. 1) to the phase plane of linear dynamics (Fig. 2).

For $l_M/\xi = 10$, $\epsilon_A = 20$ and $\epsilon_B = 8$ the modes $n = 2, 4, 6$ are in the regime of saddle instability (Fig. 2). The fundamental of the stationary wave of nonlinear dynamics corresponds to the mode $n = 4$ (Fig. 1). For $\epsilon_B = -8$ the mode $n = 2$ is

distinctly within the regime of saddles (Fig. 2). The fundamental of the stationary wave corresponds to $n = 2$ (Fig. 1). In the regime of saddle instability the nonlinear system exhibits bistability such that the sign of the symmetrical initial perturbation defines the location of the maximas and minimas of the stationary wave. For $\epsilon_B = -20$ the modes $n = 2, 4$ are in the regime of node instability (Fig. 2). The nonlinear system approaches a limit cycle (Fig. 1). The pattern of autonomous switching is reminiscent of the bistability of the saddle. Phase-locked coupling to modes of high order gives rise to sharp peaks of the quasistationary phases and of the propagating pulses. For $\epsilon_B = -100$ a single mode $n = 2$ is in the regime of focus instability (Fig. 2). The influence of fast relaxing higher modes is weak. The system exhibits a harmonic vibration of a standing wave (Fig. 1).

For short time constants of the B-channels the range of instability of foci and nodes shrinks (reduced inclination of the line $\mathrm{Tr} = 0$ in Fig. 2). Concomitantly the oscillatory solutions are suppressed. In case of $\tau_B < \tau_A$ the roles of A- and B-channels are reversed. For high values of ϵ_A the wavelength of the patterns becomes shorter with sharper peaks. Propagating droplets exhibit the character of solitons bouncing forth and back in the cable. Note, that the Eqns. 1–3 are prone to deterministic chaos. For low values of ϵ_A, very negative values of ϵ_B or low values of l_M/ξ all modes are shifted into the range of stability ($\mathrm{Tr} < 0$, $\Delta > 0$). Patterns are not induced by small inhomogeneities. In membranes of arbitrary shape (e.g. spheres, ellipsoids) the features of the dissipative patterns are found to be analogous – mutatis mutandis.

The conditions of structural instability of the fluid mosaic are not very stringent. Selforganization occurs above $P_A = 4$ i.e. above a drive parameter $\epsilon_A = 4$ in case of $\alpha_A = \alpha_B = 0.5$ in the limit $q = 0$. Differences of reversal potentials of 100 mV are quite common in cells. Electrophoretic charges of membrane proteins of $5e_0$ have been observed [8]. Thus $\epsilon_A = 20$ is certainly within the competence of natural membranes. The time constant $\tau_A = \xi^2/D_A$ is in the order of minutes for a diffusion coefficient $D_A = 1\ \mu m^2/s$ in a fluid bilayer [9] at a length constant $\xi = 10\ \mu m$. The condition of adiabatic relaxation of the potential is met safely at an electrical time constant $\tau_V = 1$ ms. The lower mobility of B-channels may be attained by interaction with the cell skeleton.

In a biological membrane the coherent patterns of channels and of potential may be of direct functional relevance in developing or adult cells or they may play a role as morphogenetic fields [10,11] inducing intracellular differentiation. The structural instability is controlled by isotropic global parameters as by the activity of ion pumps (reversal potential in the drive parameters), by chemical gating (fractions of conductivity) and by growth (wavenumber of the eigenmodes). Pattern formation is triggered by intrinsic fluctuations.

The dissipative structures in membranes as described in the present paper are a physical consequence of concepts which are generally accepted. Arbitrary mechanisms or parameters are not invoked. The formulation is restricted to the model of an ideal fluid mosaic of charged channels. In a real membrane short range interactions of the proteins are involved, of course. The ideal model provides explicit relations for the control of patterns by electrogenic activity, by channel gating and by cellular growth which may be tested by experiments in natural and reconstituted membranes.

References

1 Singer, S.J. and Nicolson, G.L. (1972) Science 175, 720–731.
2 Hladky, S.B. and Haydon, D.A. (1970) Nature 225, 451–453.
3 Neher, E. and Sakmann, B. (1976) Nature 260, 779–802.
4 Jaffe, J.F. (1977) Nature 265, 600–602.
5 Poo, M. and Robinson, K.R. (1977) Nature 265, 602–605.
6 Fromherz, P. (1988) Proc. Natl. Acad. Sci. USA, in press.
7 Hodgkin, A.L. and Huxley, A.F. (1952) J. Physiol. 117, 500–544.
8 Ryan, T.A., Myers, J., Holowka, D., Bairds, B. and Webb, W.W. (1988) Science 239, 61–64.
9 Peters, R. and Cherry, R.J. (1982) Proc. Natl. Acad. Sci. USA 79, 4317–4321.
10 Wolpert, L. (1969) J. Theor. Biol. 25, 1–47.
11 Crick, F. (1970) Nature 225, 420–422.
12 Fromherz, P. (1988) Ber. Bunsenges. Phys. Chem., in press.